

# Cooling of Photovoltaic Cells

Bryce Cruey

Jordan King

Bob Tingleff

December 7, 2006

# Contents

<b>List of Figures</b>	<b>ii</b>
<b>List of Tables</b>	<b>ii</b>
<b>1 Introduction</b>	<b>2</b>
<b>2 Objectives and Constraints</b>	<b>2</b>
<b>3 Literature Review</b>	<b>4</b>
3.1 Concentrated illumination . . . . .	4
3.2 Electrical efficiency . . . . .	5
3.3 Hybrid PV/Thermal (PV/T) systems . . . . .	6
3.3.1 Duct cooling . . . . .	7
3.3.2 Cooling by the Addition of Fins . . . . .	9
<b>4 Problem Development</b>	<b>10</b>
<b>5 Model Development</b>	<b>14</b>
5.1 Energy Balance . . . . .	14
5.2 Radiation Transmission . . . . .	15
5.3 Thermal Heat Transfer Coefficient-Natural Convection . . . . .	16
5.4 Thermal Heat Transfer Coefficient-Forced Convection . . . . .	17
5.5 One Dimensional Heat Transfer in a Fin . . . . .	18

5.6 Galerkin Finite Element Solution . . . . .	22
<b>6 Computer Algorithm</b>	<b>26</b>
<b>7 Results and Discussion</b>	<b>27</b>
<b>8 Conclusions</b>	<b>32</b>
<b>Appendix 1</b>	<b>33</b>
A.1.1 Analytical Solution Derivation . . . . .	33

## List of Tables

1	Table of Nomenclature . . . . .	1
4.1	model parameters . . . . .	11
5.1	Finite element basis function descriptions. . . . .	24

## List of Figures

2.1	PV panel with fins and duct . . . . .	3
4.1	PV panel with fins and duct . . . . .	10
	(a) Panel with fins and duct assembly. . . . .	10
	(b) Layers and fin assembly. . . . .	10
4.2	Equivalent thermal circuit to the system described in Figure 4.1. . . . .	12
5.1	Nodal breakdown of the fin shown in Figure 4.1. Elements in the region are described by $e_1 \cdots e_n$ and nodal points are described by $n_1 \cdots n_n$ . . . . .	24
6.2	Computer flow diagram detailing the progression of events for the solution to the heat transfer in the PV system. . . . .	26
7.1	Effect of Single Parameter Change on Panel Efficiency and Cell Temperature	28
	(a) Cooling Fluid Velocity . . . . .	28
	(b) Fin Thickness . . . . .	28
	(c) Fin Spacing . . . . .	28
	(d) Fin Length . . . . .	28
7.2	Effect of Single Parameter Change on Panel Power and q Duct . . . . .	30

(a)	Cooling Fluid Velocity . . . . .	30
(b)	Fin Thickness . . . . .	30
(c)	Fin Spacing . . . . .	30
(d)	Fin Length . . . . .	30
7.3	Effect of Solar Concentration on Panel Operation . . . . .	31
(a)	Panel Efficiency and Cell Temperature . . . . .	31
(b)	Panel Power and q Duct . . . . .	31
7.4	Effect of Fin Material Conductivity on Panel Operation . . . . .	32

## **Abstract**

The cooling of a photovoltaic panel via fins and a duct attached to the rear surface of the panel is investigated. Forced convection through the duct is assumed. A model is developed which allows study of the effects of varying fin parameters on panel electrical output and potential useful heat output. Electrical output is found to vary weakly with fin material and thickness, and strongly with fin length and air velocity in the duct. The model suggests a maximum value of solar concentration for a given air velocity in the duct.

## Nomenclature

Table 1: Table of Nomenclature

Symbol	Description	Units
$q_{convf}$	convective heat flux through front of panel	$(W/m^2)$
$q_{radf}$	radiative heat flux through front of panel	$(W/m^2)$
$q_{cg}$	heat flux through glass and front half of PV cell	$(W/m^2)$
$q_{cs}$	heat flux through back half of PV cell to rear surface of panel	$(W/m^2)$
$q_{fin}$	heat flux through fin	$(W/m^2)$
$q_{radb}$	radiative heat flux through rear surface of panel	$(W/m^2)$
$q_{convb}$	convective heat flux through rear surface of panel	$(W/m^2)$
$\bar{h}$	average convective heat transfer coefficient	$(W/m^2 \cdot K)$
$T_g$	glass surface temperature	$(K)$
$T_c$	PV cell temperature	$(K)$
$T_s$	panel rear surface temperature	$(K)$
$T_{ef}$	front environment temperature	$(K)$
$T_{eb}$	back environment temperature	$(K)$
$T_r$	surface opposite to rear panel surface temperature	$(K)$
$\sigma$	Stefan-Boltzman constant	$(5.67 \times 10^{-8} W/m^2 K^{-4})$
$v_w$	wind velocity	$(m/s)$
$k$	thermal conductivity	$(W/m^2 K)$
$R_{gc}$	thermal resistance from glass through top half of cell	$(m^2 K/W)$
$R_{cs}$	thermal resistance from midpoint of cell through substrate	$(m^2 K/W)$
$\epsilon$	surface emissivity	unitless
$L_{fin}$	fin height	$(m)$
$t_{fin}$	fin thickness	$(m)$
$w_{fin}$	fin length	$(m)$
$\Delta S_f$	fin spacing	$(m)$
$A$	area of panel	$(m^2)$
$I, I_2$	solar irradiance	$(W/m^2)$
$P_e$	electrical power	$(W/m^2)$
$\overline{N_u}$	Nusselt Number	None
$\overline{P_r}$	Prandtl Number	None
$\overline{R_a}$	Rayleigh Number	None
$\overline{G_r}$	Grashof Number	None
$\beta$	$1/T$	$K^{-1}$
$\nu$	Kinematic Viscosity	$m^2/s$
$\alpha$	Adsorptivity of the surface material	None
$R_e$	Reynolds Number	None

# 1 Introduction

The cooling of photovoltaic (PV) cells is a problem of great practical significance. The usable energy produced from solar energy displaces energy produced from fossil fuels, and thereby contributes to reducing global warming. However, the high cost of solar cells is an obstacle to expansion of their use.

PV cooling has the potential to reduce the cost of solar energy in three ways. First, the electrical efficiency of PV cells decreases with temperature increase. Cooling can improve the electrical production of standard flat panel PV modules. Second, cooling makes possible the use of concentrating PV systems. Cooling keeps the PV cells from reaching temperatures at which irreversible damage occurs, even under the irradiance of multiple suns. This makes it possible to replace PV cells with potentially less expensive concentrators. Finally, the heat removed by the PV cooling system can be used for building heating or cooling, or in industrial applications.

## 2 Objectives and Constraints

The objective here is to investigate a technologically straightforward means of cooling a standard PV panel. The constraints specified at the outset were that the technology be relatively inexpensive, that it would involve modifications to a standard PV panel, that useful heat could be recovered, and that it would allow for low level concentration factors (less than 5X). The goal is to develop a model that allows a sensitivity analysis of basic parameters. A specific design is not derived, as cost parameters were not investigated.

The method of cooling investigated is fins attached to the rear face of the panel. The rear surface of the panel is a substrate such as aluminum or copper. The fins are modeled as being an extension of this substrate. The substrate material is soldered or attached with adhesive to the rear surface of the cells. Values for thermal conductivity are taken from the

literature. In addition, a rectangular duct is attached to the rear surface of the panel, as shown in Figure 2.1. The duct allows air to be blown across the rear surface of the panel and potentially captured and used.

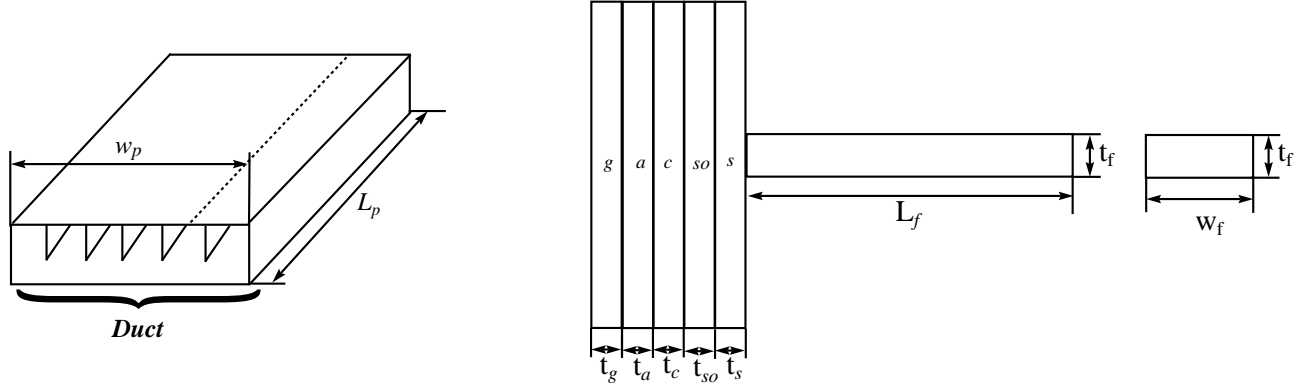


Fig. 2.1: PV panel with fins and duct

Parameters of the system that are varied are fin thickness, fin height, fin material, air velocity, and solar concentration. Outputs of the model are cell temperature, cell efficiency, electrical output, and energy leaving the system through the duct. Constants of the system are panel element thicknesses and conductivities, and the ambient temperature.

## 3 Literature Review

### 3.1 Concentrated illumination

Royne et al. (2005), in a review of PV cooling methodologies, for use under concentrated illumination, provide a set of requirements for cooling techniques. The cooling method needs to ensure that the operating temperature does not exceed the point at which irreversible degradation occurs in the cell. In addition, it is desirable for the temperature to be uniform across the cells, for the technology to be reliable and simple, for the thermal energy produced to be useable, for the pumping power to be minimal, and for the cooling technology to be efficient in the use of materials. The authors note that there is an inherent conflict in the desire to keep the temperature low to enhance electrical efficiency, and to have a high temperature, thereby increasing the usefulness of the thermal energy.

These authors define three basic geometries of concentrated PV systems: 1. Single-cell point focus; 2. A linear row of cells; 3. Densely packed cells. Royne et al. (2005) found that for a single cell geometry, passive cooling with natural convection could theoretically be used at concentrations up to  $1000\times$ , with a cell diameter around 5mm. In a linear arrangement, passive cooling could be used for concentrations of 10 or 20 suns. Heat pipes can also be used in this configuration. At higher concentrations forced convection with air or water is required, with air circulation becoming too costly at higher concentrations, and water preferred. In densely packed configurations, active cooling is required. Micro-channels etched in the silicon for water transport can reportedly maintain a temperature of  $40^{\circ}\text{C}$  under an irradiance of  $500\text{ kW/m}^2$ . Other techniques include impinging jets, submerging the cells in liquid, boiling the coolant, and coolant channels in thermal contact with the cells.

Depending on the application, the average heat transfer coefficient can be used (the ratio of the rate of heat removal to average temperature difference), or it may be necessary to use local heat transfer coefficients (Royne et al., 2005). An average coefficient can be taken from the literature, or it may be necessary to model its variation with temperature.

In their review, Royne et al. (2005) found that it was common to model heat transfer through the panel as a series of thermal resistances, with separate resistance values for cover glass, adhesive, PV cell, solder, and substrate. A linearized version of the heat transfer due to radiation is used, in which the flux varies with the fourth power of the ambient temperature, and the first power of the surface temperature.

Sala (1989) presents a theoretical overview of cooling PV cells under concentration in conditions of still air at 25°C. He finds that, without concentration, if a cell can radiate from both faces, radiation alone is sufficient to cool the cell. He also finds that natural convection alone would lead to a temperature increase of 72.5°C with no concentration, and an increase of 974°C with 10× concentration. Forced convection with air as the coolant could limit the theoretical temperature increase to 282°C at 10× concentration. If water cooling is used, temperature increases of 18°C at 100×, and 189°C at 1000×, are possible with the flow fully turbulent. Sala further finds that, considering either radiation or convection alone, if the radiation (or dissipating) surface area is twice the size of the cell area times the effective concentration, concentrations of 200× are possible while maintaining temperatures within the range in which the electrical efficiency is equal to or better than the reference efficiency. When radiation and convection are combined, Sala finds that with stagnant air, and ignoring albedo radiation, radiative losses account for up to 60% of the heat removal. With wind speed of 2m/s the losses from radiation can be 30% of the total.

### **3.2 Electrical efficiency**

A typical value for PV efficiency loss with temperature is 0.5%/°C (SEI, 2004), though this varies with the type of cell. Sala (1989) notes that the rate of reduction with temperature decreases with concentration. Tripanagnostopoulos et al. (2001) argue that, in a standard PV module, the improvements in electrical efficiency alone cannot justify the costs of the cooling system, and that cooling is only cost effective if concentration is used, or if the energy recovered through cooling is put to use.

Krauter (2004) investigated a method of reducing reflection which also provided cooling - replacing the front glass surface with a thin (1mm) film of water running over the face of the panel. He notes that the refractive index (1.3) of water is superior to that of glass. Reflective losses in glass can lead to losses in yield of 8-15%. The water decreased cell temperatures up to 22°C. The improved optics and cell temperatures increased electrical yield 10.3% over the day (8-9% after accounting for pumping energy). He also noted an unexpected aesthetic benefit.

Meneses-Rodriguez et al. (2005) considered a novel technique to improve the electrical efficiency with cooling. The authors explored the benefits of running PV cells at near their maximum theoretical temperatures (100-170°C). Theoretically, the electrical efficiency can be in the range 10-16%. The cooling fluid would be used to run a Stirling engine. With a sink temperature of 30°C, the authors estimate a theoretical total efficiency greater than 30%.

### **3.3 Hybrid PV/Thermal (PV/T) systems**

Vokas et al. (2005) investigated PV/T systems. They studied the thermal energy benefits of a thermal collector with a PV laminate attached to the front. They found the theoretical efficiency of the system was 9% lower than that of conventional thermal collectors. They estimate that a 30m<sup>2</sup> collector of this type would provide 54% of the heating and 32% of the cooling of a typical house in Athens.

Tripanagnostopoulos et al. (2001) also investigated hybrid PV/Thermal (PV/T) systems. In a PV/T system, the thermal energy is put to use – typically for space heating, water pre-heating, ventilation, or for industrial applications such as food drying. They experimented with water cooling, with channels attached to the rear surface of the PV module, with an air cooling duct, and with additional glazing on the front surface of the PV module to increase heat retention. They note that the contact between the copper sheet and pipes is a crucial aspect of the design. Thermal efficiency is calculated as the ratio of the heat carried away by the convecting fluid to the input insolation. In addition, flat, diffuse reflectors were

used to concentrate additional illumination onto the panel, yielding a concentration factor of up to 1.5. They found that while the glazing increased the thermal efficiency up to 30%, there were 16% losses in electrical efficiency due to optical effects. The reflectors, at  $1.3\times$ , increased electrical output by 16%. The water was more effective at removing heat than the air, achieving thermal efficiencies of 71%, compared with 59% for the air coolant. They note that the enhanced electrical efficiency (up to 3.2%) is not cost-effective unless the thermal energy is also used.

The thermal efficiency equations of Duffie and Beckman (1991) for solar collectors can be used to evaluate the thermal performance of a PV panel. These authors derive the useful energy gain of a collector as a linear relationship of the temperature difference between inlet fluid temperature and ambient temperature, and a collector heat removal factor.

Another well-known technique for thermal analysis of flat plate solar collectors is the Hottel-Whillier (HW) method. Duffie and Beckman (1991) set forth the general assumptions of the model and describe its usefulness in terms of relevant energy coefficients calculated from simplified mathematics. The model depicts convection, conduction, and radiation as resistive elements combined in series and parallel to form the overall heat loss coefficients for a solar collector. The pertinent equations are based on the temperature gradient between parallel plates, thermal conductivities, emissivities, and collector plate dimensions. The use of the Hottel-Whillier model is substantiated for conventional collector design by de Winter (1990). The model is extended by Florschuetz (1976) to the analysis of a combined photovoltaic/thermal collector system. This extension preserves the general form of the HW model by modifying existing model parameters to incorporate electrical output. The modifications of the original equations are based on the assumption that cell efficiency decreases linearly with increasing local temperature.

### **3.3.1 Duct cooling**

In addition to the study cited above, a number of other authors investigated cooling of a flat panel PV module with a duct thermally attached to the rear face of the module. Forced

or natural convection can be used. Fins and other additional elements can be used within the duct. This method can be incorporated into building-integrated PV, with an air space behind the PV module, and the heat captured and put to use within the building (Figure 2.1).

Brinkworth and Sandberg (2006) analyzed cooling of a PV module via a duct attached to its rear face. Natural convection through the duct removed heat from both the back face of the PV panel, and the opposite face, which warms through radiation from the back face. They found that, with an irradiance of  $200\text{W}/\text{m}^2$ , the duct reduced the temperature rise in the module by  $11^\circ\text{C}$  in still air, and  $14^\circ\text{C}$  in air moving at  $2\text{ m/s}$ . The authors combined Newton's law of cooling, the experimentally determined proportion of 60% of the heat removed at the top of the duct by convection (40% by radiation), reported values for the Nusselt number, and an energy balance at the top opening of the duct. For Reynolds numbers from 7000 to 20,000, they found that the optimum length to hydraulic depth ratio should range from 22 to 17. In another study (Brinkworth, 2006), the authors both experimentally and with computer modelling of the heat transfer and fluid mechanics found the optimum length to hydraulic depth ratio for the duct was around 20. They also found that netting across the ends, and the presence of structural members inside the ducts, had a net positive effect by increasing the turbulence, even at the expense of reduced air speed.

Tonui and Tripanagnostopoulos (2006) also investigated the use of an air duct attached to the rear face of a panel. They analyzed two possible improvements to the basic duct: the addition of a thin metal sheet parallel to the surface of the PV panel in the middle of the duct, and the addition of fins along the rear surface of the duct. Experimental results showed thermal efficiencies of 30% with fins, 28% with the thin metal sheet, and 25% with the basic duct. In the enhanced ducts, the increased convection losses from the additional surfaces lower the temperatures of those surfaces, thereby increasing radiation losses from the PV back face. The thin metal sheet has the additional benefit of reducing the temperature of the back wall of the duct (which is presumably in contact with a building surface). They note

that the pumping power to force air through the duct may be achieved with the improved electrical efficiency provided by the cooling.

### **3.3.2 Cooling by the Addition of Fins**

Effective heat transfer through fins has been well documented (White (1984), Segerland (1984), Chapman (1984)). The basic theory is to include a fin attachment at the base of a structure in order to increase its surface area and thereby increase the heat flux (White, 1984). The equations are those that account for both conductive and convective heat transfer and can be modeled by the convection dispersion equation in space and time (Segerland, 1984). However in an ideal solution as shown by White (1984) and many others, heat transfer through a fin can be simplified to one dimension and steady state. In this ideal case where the temperature varies in one direction, the base temperature of the fin is the temperature at the attachment or junction with what it is that is being cooled (White, 1984). This generalized approach is a good first approximation of the temperature gradient in the fin.

The convection-dispersion equation has been well studied and has been solved analytically in one dimension for a variety of different conditions (W.J. and van Genuchten, 1982). The convection-dispersion has also been solved numerically using a variety of different methods including finite elements, finite difference, quasilinearization, and probabilistic/statistical methods (Willis and Yeh (1987), Segerland (1984)).

Fins are constructed with high thermal-conductivity metals (copper, aluminum, etc.). They should be designed so that they are more than 60% efficient (White, 1984). Sizing the fins can be done optimally in cases when the total volume of the fin is held constant and only one of the physical dimensions are varied. This optimal sizing is based on maximizing the total heat transfer through the fin while holding the volume constant and changing one of the physical dimensions of the fin (Began Adrian, 1996). With that in mind cooling PV panels using fins may be an economical choice.

## 4 Problem Development

The method of PV module cooling investigated here is direct attachment of fins to the rear surface of the panel. The physical system is described by the layers making up the PV array and the attached fin on the back as seen in Figure 1(b). A duct is added for which the heat transfer parameters are based on the assumption of forced convection (1(a)). It is important to clearly define boundary conditions before this analysis can be executed. The input to the system is the solar irradiance ( $I$  in Figure 1(a)). The boundary conditions are the heat losses due to radiation and convection on the front and back ( $q_{rad_n}$ ,  $q_{conv_n}$ ), as well as the electrical power output ( $P_e$  in Figure 1(b)).

Average heat transfer coefficients for the front and rear surfaces are calculated based on standard equations. Various values of concentration are modeled, in order to predict the extent of cooling required under multiple suns.

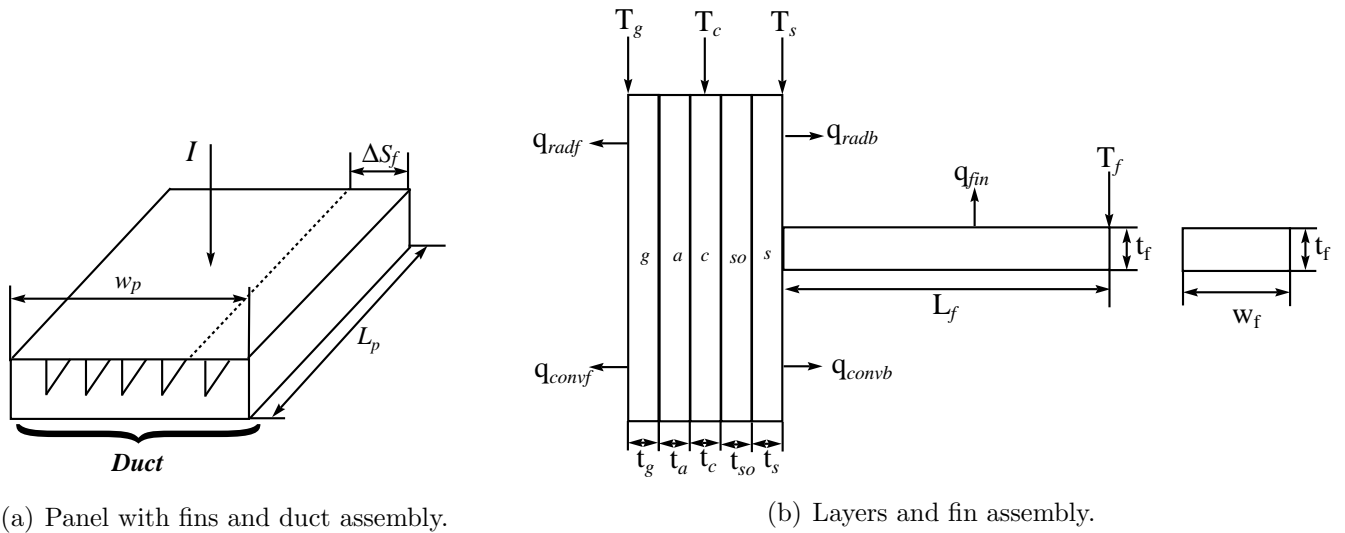


**Fig. 4.1:** PV panel with fins and duct

The model used here extends the approach of Royne et al. (2005). The PV panel is conceived as consisting of the layers shown in Figure 4.1. The layers in Figure 4.1 are described as follows:

- $g$  = Cover glass layer with thickness  $t_g$
- $a$  = Adhesive layer with thickness  $t_a$
- $c$  = Cell layer with thickness  $t_c$
- $c$  = Solder layer with thickness  $t_{so}$
- $s$  = Substrate layer with thickness  $t_s$

The fins are an extension of the substrate layer that is attached to the rear surface of the panel.

The PVCOOL model was developed to model the physical situation. The physical schematic described in Figure 4.1 (a), and (b) as it applies to our problem uses default parameters in the PVCOOL model. The thermodynamic properties of the panel, thermodynamic properties of the fin, and physical dimensions of the panel layers were held constant during throughout the experiment unless otherwise specified by the user. Default parameter values were taken from Royne et al. (2005) and are listed in Table 4.1.

**Table 4.1:** model parameters

Parameter	Value	Units	Parameter	Value	Units
$T_{ef}$	298	K	$L_{fin}$	0.2	m
$k_g$	1.4	W/m·K	$t_f$	0.02	m
$k_c$	145	W/m·K	$t_s$	$1 \times 10^{-4}$	m
$k_s$	50	W/m·K	$t_g$	$3 \times 10^{-3}$	m
$k_{fin}$	120	W/m·K	$t_c$	$12 \times 10^{-5}$	m
$k_a$	145	W/m·K	$t_a$	$1 \times 10^{-4}$	m
$\epsilon_f$	0.855		$t_{sub}$	$2 \times 10^{-3}$	m
$\epsilon_b$	0.8		$I$	1113	W/m <sup>2</sup>
$L_p$	1	m	$\rho$	0.05	
$w_f$	1	m	$U_\infty$	2	m/s
$w_p$	1	m	$\theta$	46.336	
$\Delta S_f$	0.2	m			

The electrical analogue is shown in Figure 4.2. The electrical analogy is not quite accurate since the losses through radiation and through the fin are not modeled as linear relationships. The solar radiation is modeled as penetrating the glass (after some is reflected) and striking the cell, where it is converted to electricity and heat. The heat leaves the panel through the front and rear surfaces.

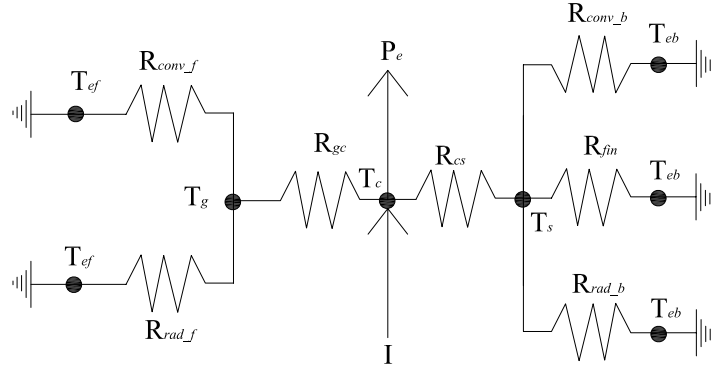


**Fig. 4.2:** Equivalent thermal circuit to the system described in Figure 4.1.

The surface emissivity of the glass is taken to be 0.855 (Royne et al., 2005). The emissivity of the rear panel surface is problematic, as emissivities for metals vary widely. The value midway between that for oxidized aluminum (0.82) and oxidized copper (0.78) is used here (0.80) (Thomas, 1999). The emissivity and absorptivity of the substrate surface were assumed to be equal for the purposes of the radiation losses.

Cell efficiency is assumed to vary with temperature according to the model proposed by (Tonui and Tripanagnostopoulos, 2006):

$$\eta_{pv} = 0.127(1 - 0.0063(T_c - 25^\circ C)) \quad (1)$$

Some assumptions are made about the temperature of the surface opposite the rear surface of the panel. In experiments with ducts attached to the back of PV modules, (Tonui and Tripanagnostopoulos, 2006) found opposite surface temperatures  $15^\circ C - 20^\circ C$  lower than the rear surface of the panel, and up to  $15^\circ C$  higher than the ambient temperature. With

an ambient temperature of  $25^{\circ}C$ , the peak opposite surface temperature was around  $12^{\circ}C$  higher than ambient, which is the assumption used here.

The air flowing across the back surface of the panel heats up as it passes over the panel. Based on the duct experiments mentioned above, an average air temperature on the back side is taken to be halfway between the ambient temperature and the opposite surface temperature. (Royne et al., 2005) assumes no radiation losses from the rear surface of the panel; the assumptions here follow the experimental results of Tonui and Tripanagnostopoulos (2006) and Brinkworth and Sandberg (2006).

## 5 Model Development

The model used in this study (PVCOOL) utilizes numerical techniques to solve the heat transfer problem described in the previous section. A finite element approximation is used to approximate the partial differential equation for heat transfer in a fin (Equation 31). Finite element approximations for the convection dispersion equation are commonly used and the method is directly applied in Segerland (1984).

The solution is based on an energy balance as shown in Equation 2 through Equation 14. Inputs to the model are physical parameters of the system such as the panel dimensions, fin dimensions, emissivities, thermal conductivities of the layers, Stefan-Boltzman's constant, and two initial guesses of what the temperature of the substrate layer is. Two initial guesses of the temperature are necessary for the secant method, which was chosen as the solution technique for this problem.

### 5.1 Energy Balance

The energy balance for the system at steady state is:

$$I = P_e + q_{radf} + q_{convf} + q_{fin} + q_{convb} + q_{radb} \quad (2)$$

Additional equations are as follows. Simplifying assumptions are used to derive the temperature of the roof, or rear surface of the duct, and the air temperature in the duct. The other equations describe energy leaving the system through radiation or convection (with a term for convection from the fin), and the conduction equations through the panel. The key to solving the system of equations is that the energy leaving the system from the top of the panel is equal to the energy conducted through the top of the panel, and similarly for the

bottom of the panel. Additional energy leaves the system in the form of electricity.

$$T_r = T_{ef} + 12^\circ C \quad (3)$$

$$T_{eb} = (T_r + T_{ef})/2 \quad (4)$$

$$q_{radf} = \epsilon\sigma(T_g^4 - T_{ef}^4) \quad (5)$$

$$q_{convf} = \frac{T_g - T_{ef}}{R_{conv}} \quad (6)$$

$$\eta_{pv} = 0.127(1 - 0.0063(T_c - 25^\circ C)) \quad (7)$$

$$P_e = \eta_{pv}I \quad (8)$$

$$q_{convb} = \frac{T_s - T_{eb}}{R_{conv}} \quad (9)$$

$$q_{radb} = \epsilon\sigma(T_s^4 - T_{eb}^4) \quad (10)$$

$$q_{gc} = q_{radf} + q_{convf} \quad (11)$$

$$q_{gc} = \frac{T_c - T_g}{R_{gc}} \quad (12)$$

$$q_{cs} = q_{radb} + q_{convb} + q_{fin} \quad (13)$$

$$q_{cs} = \frac{T_c - T_s}{R_{cs}} \quad (14)$$

## 5.2 Radiation Transmission

Radiation from the sun reaches the solar collector and can either be absorbed, reflected, or transmitted through the contact surface. A relation for the ratio of light reflected ( $I_r$ ) to the incoming total radiation ( $I_0$ ) when passing from a medium with refractive index  $n_1$  to a medium with refractive index  $n_2$  can be written (?)

$$\frac{I_r}{I_0} = \rho = \frac{1}{2} \left[ \frac{\sin^2(\theta_2 - \theta_1)}{\sin^2(\theta_2 + \theta_1)} + \frac{\tan^2(\theta_2 - \theta_1)}{\tan^2(\theta_2 + \theta_1)} \right] \quad (15)$$

where  $\theta_1$  and  $\theta_2$  are the angles of incidence and refraction, respectively. These angles are related to the refractive indices by Snell's law

$$\frac{n_1}{n_2} = \frac{\sin \theta_2}{\sin \theta_1} \quad (16)$$

Assuming that the angle of incidence is normal to the panel surface in order to maximize the solar energy available, Equation 15 becomes

$$\rho = \frac{I_r}{I_0} = \left[ \frac{(n_1 - n_2)}{(n_1 + n_2)} \right]^2 \quad (17)$$

For the purposes of this study, it is assumed that no radiation is absorbed at the front plate surface. Therefore, all incoming radiation that is not reflected is transmitted to the silicon cell where it is absorbed.

### 5.3 Thermal Heat Transfer Coefficient-Natural Convection

The equation used for calculating the thermal heat transfer coefficient ( $\bar{h}_L$ ) on an inclined flat plane is (William (2000)):

$$\overline{Nu}_L = \frac{\bar{h}_L L}{k_f} = 0.68 + \frac{0.670 Ra_L^{1/4}}{\left[ 1 + \left( \frac{0.492}{Pr} \right)^{9/16} \right]^{4/9}} \quad (18)$$

where  $\overline{Nu}_L$  is the Nusselt Number,  $k_f$  is the thermal conductivity of the fluid, and  $L$  is the length of the side of the plane in the direction of fluid flow. The parameter  $Ra_L$  is the Rayleigh Number averaged over the length of the surface, and is the product of the Grashof ( $Gr_L$ ) and Prandtl ( $Pr_L$ ) dimensionless numbers. The Grashof Number is the ratio between buoyancy forces and viscous forces.

$$Gr_L = \frac{g \cdot (\cos \theta) \beta \cdot (T_s - T_\infty) \cdot L^3}{\nu^2} \quad (19)$$

In this equation,  $g$  is the gravitational constant,  $\beta$  is the volumetric expansion coefficient and for an ideal gas is equal to  $1/T_\infty$ ,  $L$  is the characteristic length,  $\theta$  is the angle between the zenith and the plate surface, and  $\nu$  is the kinematic viscosity of the fluid. The Prandtl Number is simply:

$$Pr_L = \frac{\nu}{\alpha} \quad (20)$$

where  $\alpha$  is the thermal diffusivity and  $\nu$  is the same as above.

This equation can be used for values of  $\theta$  between 0 and 60, and laminar flow conditions. The critical Rayleigh number is:

$$Ra_{crit} = 3 \cdot 10^5 \exp[0.136 \cos(90 - \theta)]$$

For turbulent flow ( $Ra_L > Ra_{crit}$ ) the transfer coefficient equation is

$$\overline{Nu}_L = \frac{\overline{h}_L L}{k_f} = \left[ 0.825 + \frac{0.387 Ra_L^{1/6}}{\left[ 1 + \left( \frac{0.492}{Pr} \right)^{9/16} \right]^{8/27}} \right]^2 \quad (21)$$

## 5.4 Thermal Heat Transfer Coefficient-Forced Convection

The thermal heat transfer coefficient for forced convection on the back of the panel can be calculated by rearranging the equation (Transport Handout):

$$\overline{Nu}_L = \frac{\overline{h}_L L}{k_f} = 0.664 \cdot Re_L^{1/2} \cdot Pr^{1/3} \quad (22)$$

where  $Re_L$  is the Reynolds Number.

$$Re_L = \frac{U_\infty \cdot L}{\nu} \quad (23)$$

where  $U_\infty$  is the velocity of the fluid (m/s). This equation is for laminar flow ( $Re_L < 5 \cdot 10^5$ ). For transitional flow with  $5 \cdot 10^5 < Re_L < 10^7$  the following equation can be used (Transport Handout)

$$\overline{Nu}_L = Pr^{1/3}(0.037Re_L^{0.8} - 850) \quad (24)$$

## 5.5 One Dimensional Heat Transfer in a Fin

The general derivation of one-dimensional heat transport through an extended surface is outlined by William (2000). Assuming steady state conditions, the first law of thermodynamics can be applied to a control volume, where  $q_x$  is the rate at which heat is conducted into the control volume,  $q_{x+\Delta x}$  is the rate of heat conduction out of the control volume, and  $dq_c$  is the heat lost from the surface area due to convection.

$$\begin{pmatrix} \text{Rate of energy} \\ \text{conducted into} \\ \text{control volume} \end{pmatrix} = \begin{pmatrix} \text{Rate of energy} \\ \text{conducted out of} \\ \text{control volume} \end{pmatrix} + \begin{pmatrix} \text{Rate of energy} \\ \text{convected away} \\ \text{from control volume} \end{pmatrix}$$

in equation form:

$$q_x = q_{x+\Delta x} + dq_c \quad (25)$$

or

$$q_x = \left( q_x + \frac{dq_x}{dx} dx \right) + dq_c \quad (26)$$

simplifying yields

$$-\frac{dq_x}{dx} dx = dq_c \quad (27)$$

the conduction term in this equation (left hand side) can be replaced by Fourier's law

$$q_x = -kA \frac{dT}{dx} \quad (28)$$

where  $k$  is the thermal conductivity and  $A$  is the cross-sectional area of the fin. Differentiating with respect to  $x$  gives;

$$\frac{dq_x}{dx} = -k \frac{d}{dx} \left( A \frac{dT}{dx} \right) \quad (29)$$

The convective term in equation 27 can be replaced with Newton's law of cooling.

$$dq_c = \bar{h}_c dA_s (T - T_\infty) \quad (30)$$

where  $A_s$  is the surface area of the fin and  $T_\infty$  is the temperature of the ambient air. substituting equations 29 and 30 into equation 3 gives

$$k \frac{d}{dx} \left( A \frac{dT}{dx} \right) dx = \bar{h}_c dA_s (T - T_\infty) \quad (31)$$

dividing out  $k$  and differentiating the left hand side gives

$$\frac{dA}{dx} \frac{dT}{dx} + A \frac{d^2T}{dx^2} = \frac{\bar{h}_c}{k} \frac{dA_s}{dx} (T - T_\infty) \quad (32)$$

rearranging

$$\frac{d^2T}{dx^2} + \frac{1}{A} \frac{dA}{dx} \frac{dT}{dx} - \frac{\bar{h}_c}{k} \frac{1}{A} \frac{dA_s}{dx} (T - T_\infty) = 0 \quad (33)$$

letting  $\theta = T - T_\infty$

$$\frac{dT}{dx} = \frac{d\theta}{dx}$$

and

$$\frac{d^2T}{dx^2} = \frac{d^2\theta}{dx^2}$$

substituting

$$\frac{d^2\theta}{dx^2} + \frac{1}{A} \frac{dA}{dx} \frac{d\theta}{dx} - \frac{\bar{h}_c}{k} \frac{1}{A} \frac{dA_s}{dx} \theta = 0 \quad (34)$$

assuming a constant cross-sectional area

$$\frac{dA}{dx} = 0$$

The surface area for the element can be written in terms of the fin perimeter

$$Pdx = dA_s$$

or

$$P = \frac{dA_s}{dx}$$

substituting the above relations into equation 34 and letting  $n = \sqrt{\bar{h}_c P / kA}$

$$\frac{d^2\theta}{dx^2} - n^2\theta = 0 \quad (35)$$

The governing equation for heat transfer in a fin as derived in Equation 35 has been well documented as the convection dispersion equation in one dimension (Segerland (1984), William (2000), Chapman (1984), White (1984)). With assumptions about the homogeneity of the thermal conductivities, and how it varies over the cross sectional area in space, the governing equation for heat transfer in a fin can be written as:

$$k_f A_f \frac{\partial^2 \mathbf{T}}{\partial x^2} - \bar{h}_f P_f \mathbf{T} + \bar{h}_f P_f \mathbf{T}_{\mathbf{eb}} = 0 \quad (36)$$

Where

- $k_f$  = The thermal conductivity of the fin ( $W/m \cdot K$ )
- $A_f$  = the crosssectional area of the fin (in the direction of heat flow) ( $m^2$ )
- $\mathbf{T}$  = The temperature gradient of in the fin ( $K$ )
- $\bar{h}_f$  = The heat transfer coefficient of the fin ( $W/m^2 \cdot K$ )
- $P_f$  = The perimeter of the fin ( $m$ )

The perimeter and the area are described as (refer to Figure 1(b))

$$A_{fin} = t_f \cdot w_f \quad (37)$$

$$P_{fin} = 2 \cdot (t_f + w_f) \quad (38)$$

The boundary conditions for the model described in Equation 36 are a Dirichlet (Constant) temperature at the back plate of the panel and base of the fin such that:

$$T(x = 0) = T_s \quad (39)$$

There is a Nuemann flux boundary condition at the end of the fin that describes the heat loss due to convection by Newton's Law of cooling such that:

$$-kA \frac{dT}{dx} = hA(T_b - T_f) \quad (40)$$

Where  $T_b$  is the Temperature at the end of the fin.

The analytical solution to Equation 36 has been shown by many and is derived in detail in Appendix 1 using the derivation from William (2000). It is left to the reader to show that the analytical solution to Equation 36 is as follows:

$$q_{fin} = kA_f(T_s - T_{eb})\sqrt{h_f P_f/k_f A_f} \tanh(L\sqrt{h_f P_f/k_f A_f}) \quad (41)$$

## 5.6 Galerkin Finite Element Solution

Galerkin Finite element scheme is a method of solving PDEs by turning them into a system of linear equations. As in other types of methods used to do the same thing such as finite difference and linearization techniques the system is defined as an array of nodal points. However, the method of finite elements differs from a finite difference scheme, which assumes that the temperature gradient in between nodes is the arithmetic average of the two nodes surrounding it. The finite element methodology incorporates weighting or basis functions and integrates between nodes. The Galerkin Finite element technique uses the basis functions as the weighting function Table 5.1. This methodology can be applied to solving Equation 36 by piecewise defining the integrals over the entire region Equation 42.

$$I = \int_0^L N_i(x)\mathcal{L}(T)dx = 0 \quad (42)$$

where  $N_i$  is the weighted shape function or basis function. The integral in Equation 42 is piecewise defined over the entire domain of the field such that

$$I_e = \sum_{\ell} \int_0^{Le} N_i \mathcal{L}(T) dx \quad (43)$$

Where  $I_e$  is the integral of the function shown in Equation 42 for a single element. Equation 36 can be rearranged for a finite element solution in the form

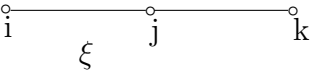
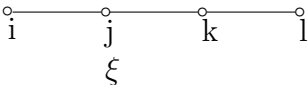
$$\mathcal{L}(\mathbf{T}) = k_f A_f \frac{\partial^2 \mathbf{T}}{\partial x^2} - h P_f \mathbf{T} + h_f P_f \mathbf{T}_{\text{eb}} = 0 \quad (44)$$

With the assumption that  $\mathbf{T}$  is a function of the basis functions (Equation 45) the integrations can be evaluated.

$$\mathbf{T} = \hat{\mathbf{T}} = \mathbf{N} \tilde{\mathbf{T}} \quad (45)$$

The  $\mathbf{N}$  vector contains the basis functions for the discretized region. The basis functions used in this model are cubic, quadratic linear (chapeau) weighting functions (Table 5.1). The basis functions are written such that there is a transformation from the global coordinate system in  $X$  and transformed to a local natural coordinate system in  $\xi$ . For the mathematics behind this transformation refer to Segerland (1984). For the remainder of this paper the basis functions will be referenced in  $\xi$ .

Table 5.1: Finite element basis function descriptions.

Type of element	Physical Model	Basis function
Linear simplex		$N_i = \frac{1}{2}(1 - \xi)$ $N_j = \frac{1}{2}(1 + \xi)$
Quadratic simplex		$N_j = 1 - \xi^2$ $N_k = \frac{1}{2}\xi(1 + \xi)$
Cubic element		$N_i = -\frac{1}{16}(1 + 3\xi)(1 - 3\xi)(1 - \xi)$ $N_j = \frac{9}{16}(1 + \xi)(1 - 3\xi)(1 - \xi)$ $N_k = \frac{9}{16}(1 + \xi)(1 + 3\xi)(1 - \xi)$ $N_l = -\frac{1}{16}(1 + \xi)(1 + 3\xi)(1 - 3\xi)$

The region of the fin is discretized into a series nodal points Figure 5.1. The elements are the spaces between the nodes to which the basis functions are applied.

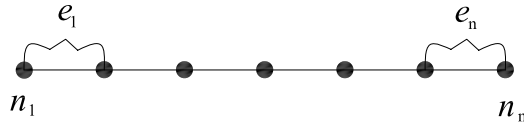


**Fig. 5.1:** Nodal breakdown of the fin shown in Figure 4.1. Elements in the region are described by  $e_1 \cdots e_n$  and nodal points are described by  $n_1 \cdots n_n$

The elemental matrix formulation utilizes Gauss Lagrange Quadrature integration to perform the integrations. The global matrix equations are formulated following the order presented in Equation 46 (For the derivation of the matrix equations, and a more in-depth description of Gauss Lagrange Quadrature refer to Segerland (1984)). It is left to the reader to refer to Segerland (1984), or Willis and Yeh (1987) for further description of the finite element solution technique and its application.

$$A, B = \begin{bmatrix} I & I & 0 & 0 \\ I & I + II & II & 0 \\ 0 & II & II + III & III \\ 0 & 0 & III & III \end{bmatrix} \quad (46)$$

## 6 Computer Algorithm

The system of equations 3 – 15, plus the heat transfer in the fins, is solved using an iterative procedure. Two initial guesses of the temperature of the substrate ( $T_s$ ) as  $T_1$  and  $T_2$  are inserted into the model to get the secant method started. The secant subroutine communicates with the the energy balance function that systematically solves Equation 2 through Equation 14. The function needs information about the heat loss in the fin from the finite element solution as well as information from the interpolation scheme described for the heat transfer coefficients for the front plate, back plate and the fin. The value of the function is checked against divergence, slow progress, and a maximum iterations criteria in secant. This process is repeated until the solution is found or the model produces unrealistic results and stops. Figure 6.2 shows the computer algorithm in detail.

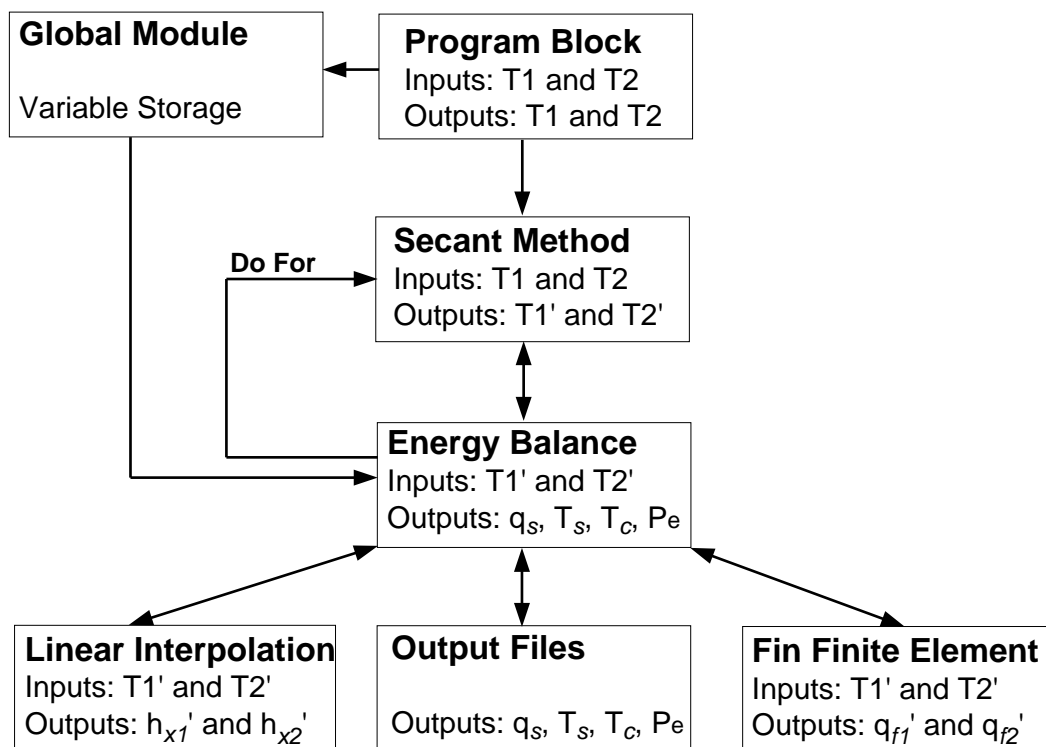


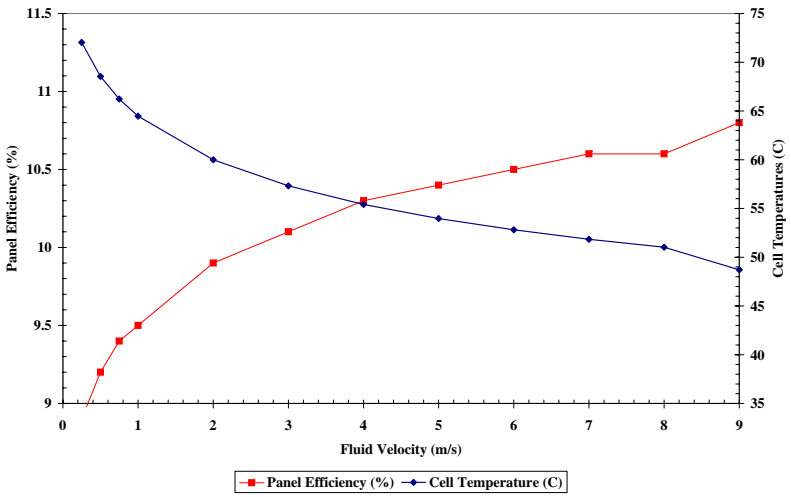
**Fig. 6.2:** Computer flow diagram detailing the progression of events for the solution to the heat transfer in the PV system.

## 7 Results and Discussion

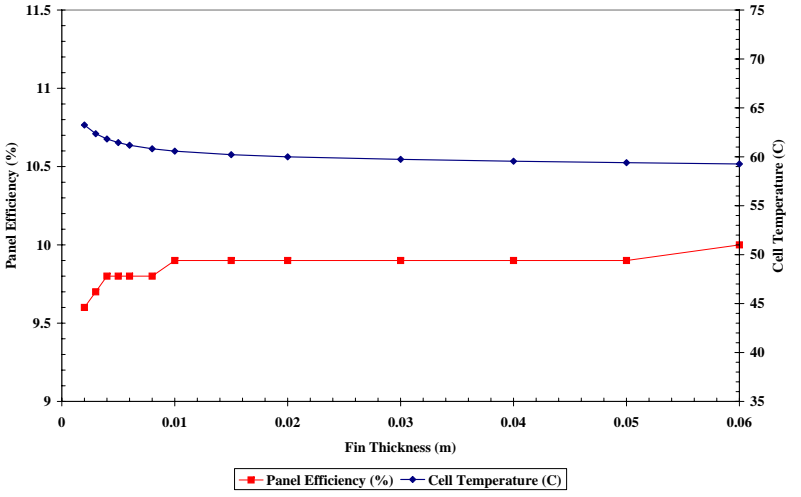
The results of this investigation show how changes in the decision variables effect the state variables of interest. To examine the effects of changing parameters that had to do with the physical system, the fluid velocity in the duct, fin thickness, fin spacing, fin material, and fin length were varied over a range of values (Figure 7.1).

It is observed in Figure 7.1 (a) that the cell temperature ( $T_c$ ) decreases as the cooling air velocity increases. This causes the panel efficiency ( $\eta_{pv}$ ) to increase. At approximately 8 m/s the flow becomes turbulent. This causes an even greater change in  $\eta_{pv}$  and  $T_c$  than observed in the laminar flow region. However, the high velocity that causes transition to turbulence cannot be reached in practice due to the greater load of the pump associated with such high speeds. The parasitic load of the cooling duct pump was not considered in this investigation. If turbulent flow conditions were able to be induced by some other means, there would be a gain in  $\eta_{pv}$ . The addition of netting over the ends of the duct, as suggested by Brinkworth (2006), has the effect of inducing turbulence and preventing birds from entering the duct.

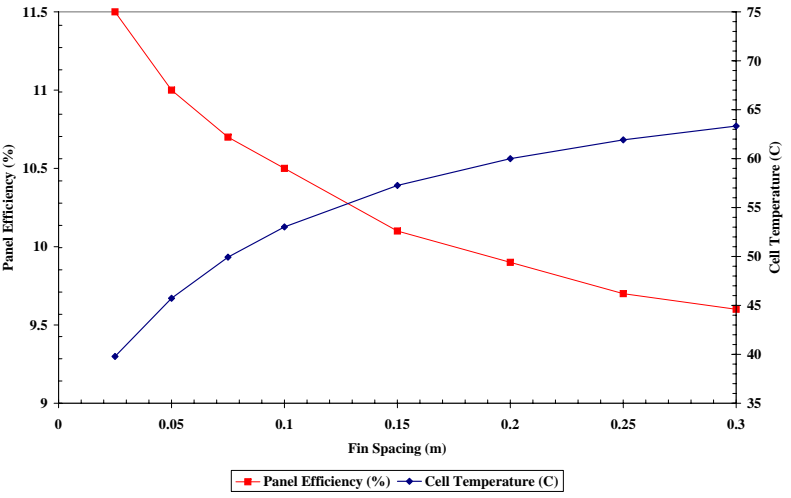
Varying the fin thickness over a range of 0-0.5m indicated that this is a parameter that has little effect on the performance of the panel (Figure 7.1 (b)). Panel efficiency only had a change over this range of 9.6 to just about 10%. This result has design application by allowing the designer to minimize materials needed for the fins.



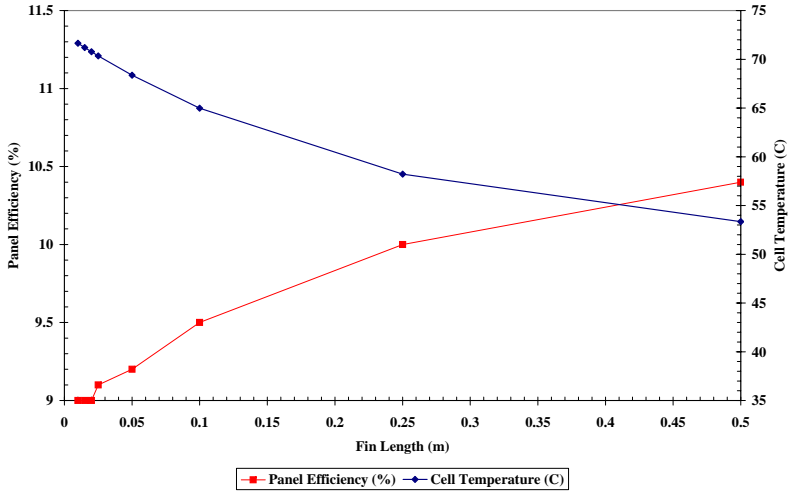
(a) Cooling Fluid Velocity



(b) Fin Thickness



(c) Fin Spacing



(d) Fin Length

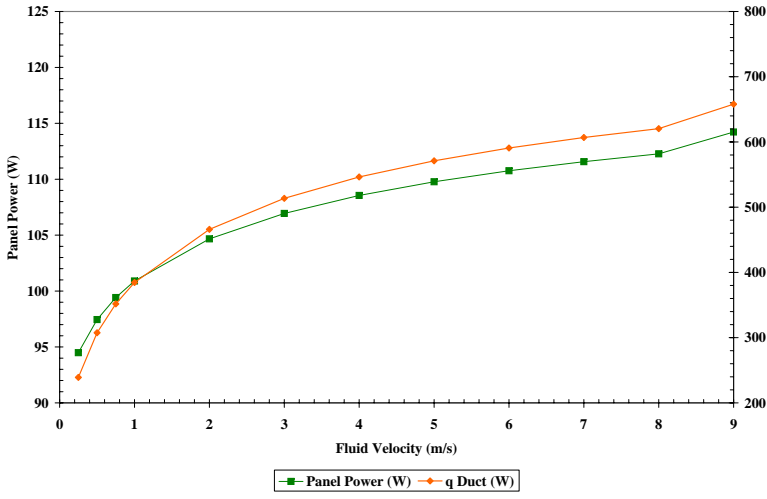
**Fig. 7.1:** Effect of Single Parameter Change on Panel Efficiency and Cell Temperature

Fin spacing (Figure 1(c)) appears to have the greatest effect on  $\eta_{pv}$  and  $T_c$ . However, these results overestimate the benefits as the fin spacing decreases. This is because the 1-d model was unable to account for overlapping thermal boundary layers that would appear between fins.

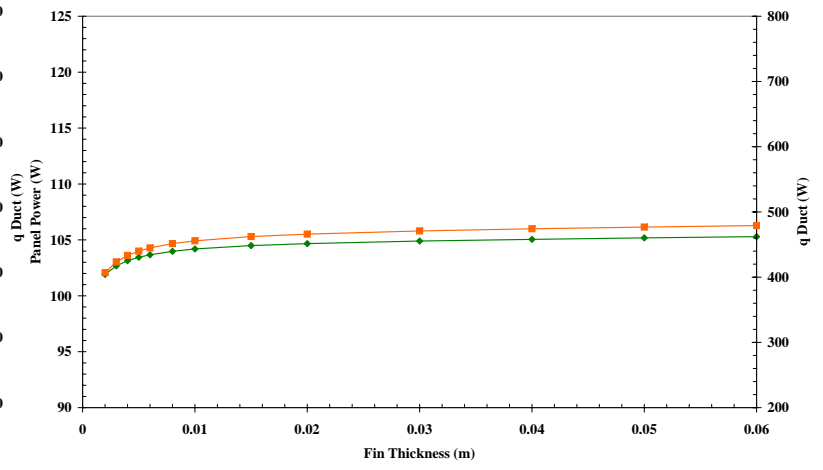
As the fin length (Figure 1(d)) increases,  $\eta_{pv}$  increases and  $T_c$  decreases. In order to use this correlation for design purposes, a maximum fin length should be set. This maximum will change depending on the system, such as applications that have a finite length on the back of the panel that the fins can occupy.

Figure 7.2 gives the change in panel power ( $P_e$ ) and heat flux into the cooling duct ( $q_{duct}$ ) as the decision variables are perturbed.

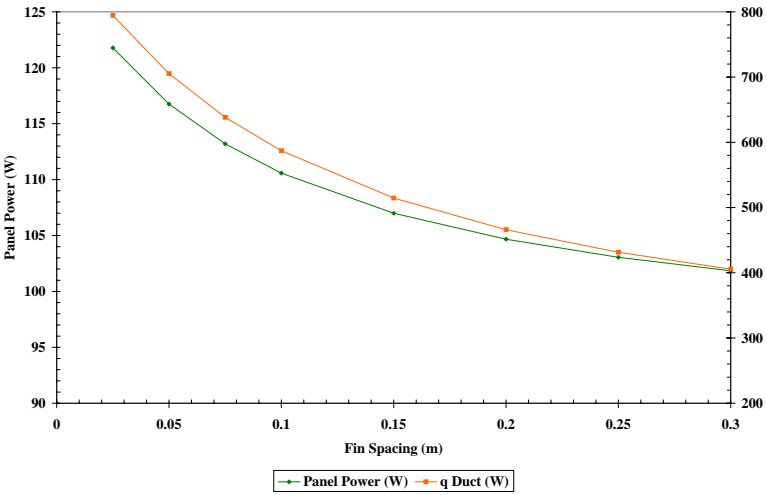
The greater the velocity of the coolant the higher  $P_e$  and  $q_{duct}$ . These results are inversely related to cell temperature. This makes sense because the heat lost from the cell layer is removed to the duct. The transition from laminar to turbulent flow conditions is also observed at 8 m/s. This supports the idea that an induced turbulent flow in the cooling duct has the potential to increase the overall power produced by the system. The fin thickness has little effect on  $P_e$  and  $q_{duct}$ . Fins that are more closely separated give the best  $P_e$ . However, the same issue appears at small spacings as was observed for  $\eta_{pv}$  and  $T_c$ . Again, the model assumptions overestimate the ability of the fins to remove heat from the panel. There is a positive correlation between fin length,  $P_e$ , and  $q_{duct}$ . Again, this means that the fin length should be maximized to the boundary of its feasible length for the given application in order to maximize panel power.



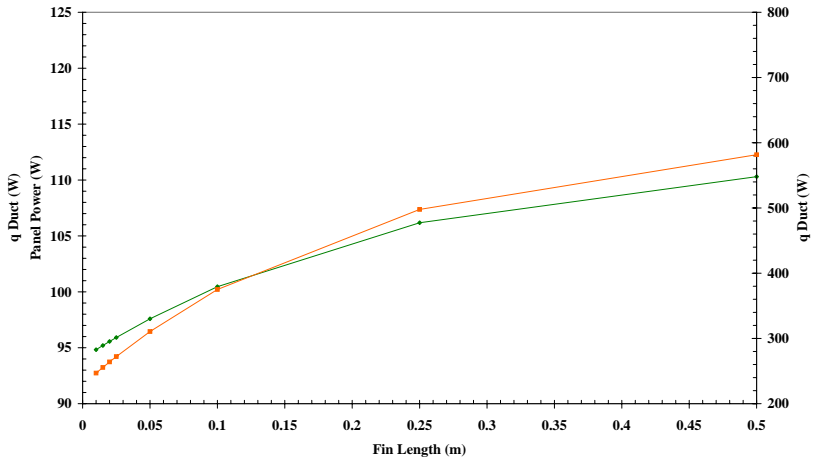
(a) Cooling Fluid Velocity



(b) Fin Thickness



(c) Fin Spacing



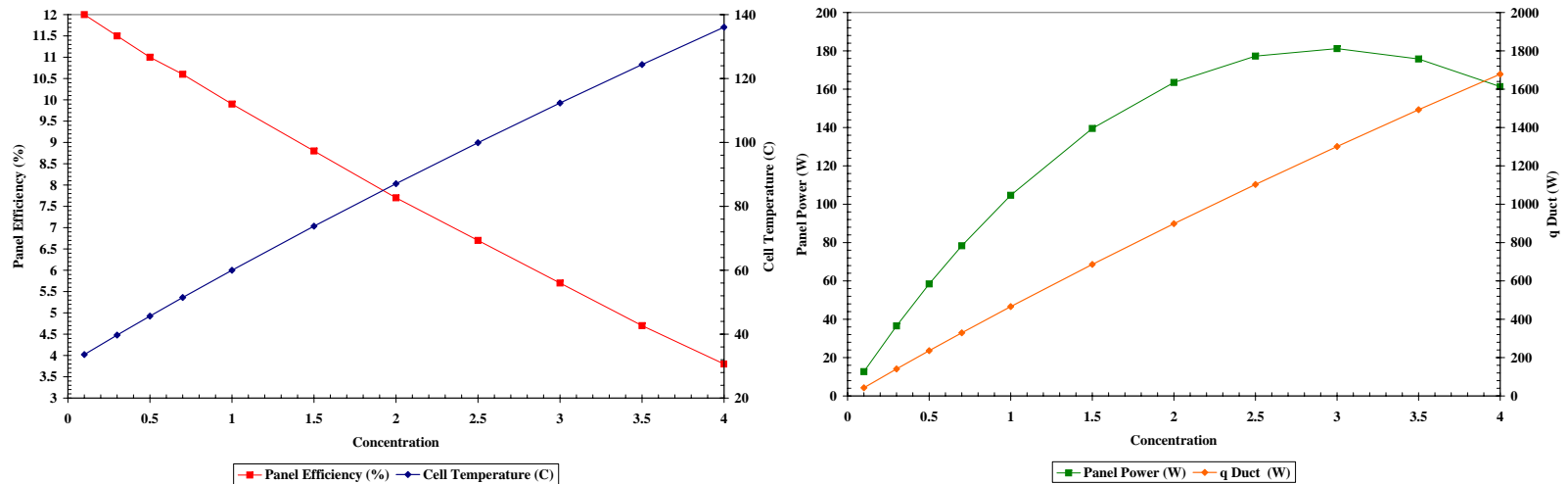
(d) Fin Length

**Fig. 7.2:** Effect of Single Parameter Change on Panel Power and q Duct

The change in the state variables observed by increasing the magnitude of incoming radiant energy with a concentrator over a range of magnitudes is given in Figure 7.3. Figure 3(a) gives the apparent relation between panel efficiency and cell temperature, which is the result of the linear equation that uses  $T_c$  to calculate  $\eta_{pv}$  (Equation 7).

In Figure 3(b) there is observed to be an optimal concentration at about 3 suns that maximizes  $P_e$ . However, this maximum falls outside of the typical operating temperature of solar panels and may cause degradation of the cell over time.

An optimization of the system could be performed given realistic limits on the decision variables. For fin thickness and length, the optimal value lies at this upper limit. The tradeoff between increased velocities of the cooling air and parasitic pump load would need to be investigated. The optimal fin width could then be set based on the other fixed parameters. Then, the optimal concentration magnitude could be determined that satisfies an upper bound on the temperature at which the cell begins to degrade.



(a) Panel Efficiency and Cell Temperature

(b) Panel Power and q Duct

**Fig. 7.3:** Effect of Solar Concentration on Panel Operation

The effect of changing the fin material can be seen in Figure 7.4. The default assumption is a fin made of aluminum nitride, with a thermal conductivity of  $120 \text{ W/mK}$ . Increasing

the conductivity above this value increases the power output of the panel less than one-half percent. Decreasing the conductivity to the range of a poor metal conductor decreases panel output one or two percent.

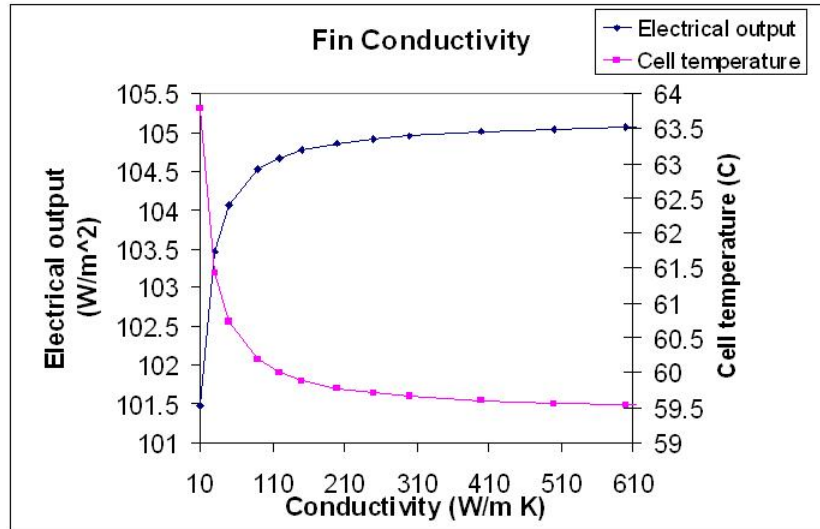


Fig. 7.4: Effect of Fin Material Conductivity on Panel Operation

## 8 Conclusions

- Induced turbulent flow in the cooling duct causes greater heat transfer from the panel, which increases the panel's electrical output and efficiency.
- Increasing the fin thickness over 1 cm has a negligible effect on panel power and efficiency.
- An optimal concentrator magnitude exists for a system with limits on the decision variables and cell operating temperature.
- Changing the fin conductivity has little impact on panel output.

# Appendix 1

## A.1.1 Analytical Solution Derivation

$$\frac{d^2\theta}{dx^2} - n^2\theta = 0 \quad (47)$$

has the general solution

$$\theta = C_1 \cosh(nx) + C_2 \sinh(nx) \quad (48)$$

Boundary conditions are  $T = T_w$  at  $x = 0$  and  $\frac{dT}{dx} = 0$  at  $x = L$  (no heat transferred across the tip). In terms of  $\theta$ , the boundary conditions are  $\theta_w = T_w - T_\infty$  at  $x = 0$  and  $\frac{d\theta}{dx} = 0$  at  $x = L$ . Applying the first boundary condition gives

$$\theta = C_1 \cosh(nx) + C_2 \sinh(nx) \quad (49)$$

$$\theta_w = C_1(1) + C_2(0)$$

$$C_1 = \theta_w$$

differentiating  $\theta$  with respect to  $x$

$$\frac{d\theta}{dx} = \theta_w n \sinh(nx) + C_2 n \cosh(nx) \quad (50)$$

applying the second boundary condition

$$0 = \theta_w n \sinh(nL) + C_2 n \cosh(nL)$$

and

$$C_2 = -\frac{\theta_w \sinh(nL)}{\cosh(nL)}$$

the solution becomes

$$\frac{\theta}{\theta_w} = \frac{\cosh(nL) \cosh(nx) - \sinh(nL) \sinh(nx)}{\cosh(nL)} \quad (51)$$

Using Fourier's law

$$q_x = -kA \frac{d\theta}{dx} \Big|_{x=0} \quad (52)$$

Equation 51 differentiated and substituted into equation 52 gives

$$\begin{aligned} q_x &= -\frac{kA\theta_w}{\cosh(nL)} * [n \cosh(nL) \sinh(nx) - n \sinh(nL) \cosh(nx)] \Big|_{x=0} \quad (53) \\ &= -\frac{kA\theta_w}{\cosh(nL)} [n(0) - n \sinh(nL)] \end{aligned}$$

simplifying

$$q_x = kAn\theta_w \tanh(nL) \quad (54)$$

and in terms of the original parameters

$$q_x = kA(T_w - T_\infty) \sqrt{\bar{h}_c P / kA} \tanh(L \sqrt{\bar{h}_c P / kA}) \quad (55)$$

## References

- Began Adrian, Michael Moran, G. T. (1996). *Thermal Design and Optimization*. John Wiley and Sons, Inc.
- Brinkworth, B. (2006). “Optimum depth for PV cooling ducts.” *Solar Energy*, 80, 1131–1134.
- Brinkworth, B. and Sandberg, M. (2006). “Design procedure for cooling ducts to minimise efficiency loss due to temperature rise in PV arrays.” *Solar Energy*, 80, 89–103.
- Chapman, A. J. (1984). *Heat Transfer*. Macmillan Publishing Company, New York.
- F. deWinter, ed. (1990). *Solar Collectors, Energy Storage, and Materials*. The MIT Press.
- Duffie, J. A. and Beckman, W. A. (1991). *Solar Engineering of Thermal Processes*. John Wiley and Sons, Inc.
- Florschuetz, L. W. (1976). “Extension of the Hottel-Whillier-Bliss model to the analysis of combined photovoltaic/thermal flat plate collectors.” *Photovoltaics and Materials*.
- Krauter, S. (2004). “Increased electrical yield via water flow over the front of photovoltaic panels.” *Solar Energy Materials & Solar Cells*, 82, 131–137.
- Meneses-Rodriguez, D., Horley, P. P., Gonzalez-Hernandez, J., Vorobiev, Y. V., and Gorley, P. N. (2005). “Photovoltaic solar cells performance at elevated temperatures.” *Solar Energy*, 78, 243–250.
- Royne, A., Dey, C. J., and Mills, D. R. (2005). “Cooling of photovoltaic cells under concentrated illumination: a critical review.” *Solar Energy Material & Solar Cells*, 86, 451–483.
- Sala, G. (1989). *Solar Cells and Optics for Photovoltaic Concentration*, 239–267. Adam Hilger, Bristol and Philadelphia.
- Segerland, L. J. (1984). *Applied Finite Element Analysis*. John Wiley and Sons, Inc., second edition.

- SEI, S. E. I. (2004). *Photovoltaics Design and Installation Manual*. New Society Publishers.
- Thomas, L. C. (1999). *Heat Transfer - Professional Version*. Capstone Publishing Corporation.
- Tonui, J. and Tripanagnostopoulos, Y. (2006). “Improved PV/T solar collectors with heat extraction by forced or natural air circulation.” *Renewable Energy*.
- Tripanagnostopoulos, Y., Nousia, T., Souliotis, M., and Yianoulis, P. (2001). “Hybrid photovoltaic/thermal solar systems, Process heating tip sheet 3.” *Pergamon*.
- Vokas, G., Christandonis, N., and Skittides, F. (2005). “Hybrid photovoltaic-thermal systems for domestic heating and cooling -A theoretical approach.” *Solar Energy*, 80, 607–615.
- White, F. M. (1984). *Heat Transfer*. Addison Wesley Publishing Company, Inc.
- William, J. S. (2000). *Engineering Heat Transfer* Second Edition. CRC Press LLC.
- Willis, R. and Yeh, W. (1987). *Groundwater Systems*. Pearson Education Inc.
- W.J., A. and van Genuchten, M. T. (1982). *Analytical Solutions of the One-Dimensional Convective-Dispersive Solute Transport Equation*. Department of Agriculture.